eJSSNT Regular Paper

e-Journal of Surface Science and Nanotechnology **23**, 188–192 (2025)

Construction of Machine Learning Potentials toward the Exploration of Alloy Cluster Catalysts

Kentaro Miyamoto,[a] Koji Shimizu,[a, b, †] Anh Khoa Augustin Lu,[a, c, d] Satoshi Watanabe [a, ‡]

[a] *Department of Materials Engineering, The University of Tokyo, 7-3-1 Hongo, Bunkyo-ku, Tokyo 113-8656, Japan*
[b] *Research Center for Computational Design of Advanced Functional Materials, National Institute of Advanced Industrial Science and Technology (AIST), 1-1-1 Umezono, Tsukuba, Ibaraki 305-8568, Japan*
[c] *Research Center for Materials Nanoarchitectonics (MANA), National Institute for Materials Science (NIMS), 1-1 Namiki, Tsukuba, Ibaraki 305-0044, Japan*
[d] *Mathematics for Advanced Materials Open Innovation Laboratory, National Institute of Advanced Industrial Science and Technology (AIST), 2-1-1 Katahira, Aoba-ku, Sendai, Miyagi 980-8577, Japan*
[†] *Corresponding author: koji.shimizu@aist.go.jp*
[‡] *Corresponding author: watanabe@cello.t.u-tokyo.ac.jp*

Received: 8 February, 2025; Accepted: 27 March, 2025; J-STAGE Advance Publication: 17 May, 2025; Published: 17 May, 2025

High entropy alloys (HEAs) are expected to show excellent performance in various fields, such as catalysts and high-temperature structural materials, but the huge number of configurations makes it difficult to find the optimal compositions for HEAs. In this study, machine learning potentials were developed to accurately predict the total and H/CO adsorption energies of multi-element slab models and cluster models of various sizes and shapes, based on density functional theory calculations.

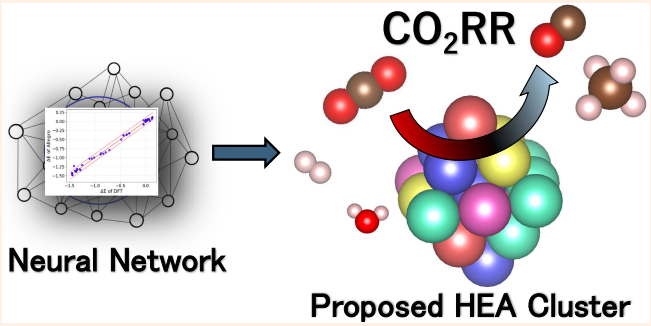

Keywords *High entropy alloys; Machine learning; Density functional theory; Catalysts; CO_2 reduction reaction*

I. INTRODUCTION

The electrochemical reduction of CO_2 (CO_2RR) is gaining increasing attention as a key technology for achieving a sustainable society. However, its practical implementation remains challenging due to the high thermodynamic stability of CO_2, which requires substantial energy input for its reduction. Additionally, CO_2RR involves multiple reaction pathways, yielding a variety of hydrocarbon compounds, including formic acid, formaldehyde, methanol, methane, acetic acid, and ethanol. Suppression of the hydrogen evolution reaction (HER), a major side reaction, is also important, because it significantly reduces the Faraday efficiency. Effectively controlling these reaction pathways requires the development of highly active and selective CO_2RR catalysts. Copper (Cu) is widely recognized as a promising CO_2RR catalyst [1] due to its balanced adsorption energies for both hydrogen (H) and carbon monoxide (CO), which are essential for facilitating hydrocarbon formation. Effective catalysts must weakly adsorb H atoms to suppress HER while maintaining appropriately strong CO adsorption to promote the conversion to highly reduced hydrocarbon products [2]. However, the search for more efficient CO_2RR catalysts remains crucial, as Cu requires high overpotentials to effectively drive CO_2RR [3].

High-entropy alloy (HEA) catalysts show great promise in addressing the challenges of CO_2RR. The concept of HEAs was introduced by Cantor *et al.* [4] and Yeh *et al.* [5], defining them as single-phase solid solutions composed of five or more elements in relatively equal concentrations (5–35 at%). Recent studies have highlighted numerous HEAs with properties superior to conventional alloys [6], increasing the expectations for their potential to enhance material functionality. On the other hand, identifying HEAs designed for specific applications remains challenging due to the vast number of compositions and configurations. To date, only a small fraction of the potential composition space has been explored, suggesting that many more highly functionalized HEAs are yet to be discovered.

Optimizing the shape and size of the catalyst also im-

proves its activity and selectivity. Nanoparticle catalysts exhibit distinct properties from bulk metals due to their high surface area-to-volume ratios and pronounced quantum size effects [7]. Various mono-elemental nanoparticles, including Ag, Au, Cu, Ni, and Pd, have demonstrated enhanced CO_2RR activity [8]. In terms of size, smaller nanoparticles often exhibit higher catalytic activity [7], and sub-nanoclusters with fewer than ~30 atoms have shown significantly better performances [9]. On the other hand, catalytic activity can diminish below a certain size [10], indicating that a complex relationship between size and catalytic performance. Regarding shapes, superior catalytic activity is often attributed to low-coordinated surface sites, such as edges, which are abundant in small nanoparticles [11]. The (111) surface has been reported to increase H adsorption energy [12], and Au nanoparticles with an octahedral shape, which consists of (111) facets, have demonstrated high CO_2RR activity [7]. By carefully tuning their size and shape, nanoparticle catalysts can achieve superior catalytic performance.

Experimentally screening potential catalysts one by one is both time-consuming and costly. In this regard, computational simulations can be used to accelerate the search by both reducing the cost and accelerating the process. First-principles calculations based on density functional theory (DFT) are a powerful method for accurately predicting physical properties, and in recent years, databases of DFT calculation results have expanded rapidly. However, DFT calculations are computationally intensive, and despite the large amount of available data, most results are derived from ideal crystal structures consisting of a limited number of elements. In particular, data on HEAs and nanoclusters remains scarce. Given these limitations, developing methods that achieve DFT accuracy with lower computational costs is highly desirable. In this context, machine learning potentials (MLPs) have emerged as a promising approach, with interatomic potentials based on neural networks gaining increasing attention in recent years [13, 14].

In this study, MLPs are developed to pave the way toward the design of HEA cluster catalysts for the CO_2RR. Since the activity and selectivity of this reaction are highly correlated with the adsorption energies of CO molecules and H atoms, the MLPs were trained to predict these values. By incorporating training datasets of octahedral cluster models with various structural features (vertices, edges, faces, etc.), catalytic performance on uneven surfaces is also explored.

II. COMPUTATINAL DETAILS

A. First-principles calculations

DFT calculations of optimized structures, total energies, and adsorption energies were used as training data for MLPs, focusing on nine elements (Ag, Au, Co, Cu, Ni, Ir, Pd, Pt, and Rh) that are promising as catalysts. The datasets used in this study include not only those calculated in our laboratory but also those obtained from previous studies [2, 15] and the novel materials discovery (NOMAD) database [16].

Structure optimization calculations were conducted for models with different atomic configurations in bulk face-centered cubic (FCC) crystals (8 atoms per supercell) containing up to 5 of the nine elements, as well as in octahedral clusters (19 and 44 atoms) containing up to 4 of the nine elements. Octahedral clusters have various structural features, such as vertices, edges, and faces, which were incorporated into the training data to investigate the unique catalytic performance of uneven surfaces. Additionally, structure optimizations were performed for several unary models with varying shapes and sizes, as detailed later in Section III.C.

For the in-house dataset, the DFT calculations were performed using the vienna *ab initio* simulation package (VASP) [17]. The exchange-correlation functional was based on the generalized gradient approximation (GGA) with Perdew-Burke-Ernzerhof (PBE) [18]. The projector-augmented-wave (PAW) method [19] was used for the interaction between inner-shell electrons and nuclei. A cut-off energy of 500 eV was used, and k-point samplings of $10 \times 10 \times 10$ and $3 \times 3 \times 3$ were used for the bulk and cluster models, respectively, based on the Monkhorst-Pack scheme [20]. The atomic configurations were relaxed until the atomic forces were reduced to below 0.01 eV Å^{-1}.

DFT calculations for alloy slab models with 1 to 5 elements, including adsorbed H atoms and CO molecules, were obtained from the dataset of previous studies [2, 15]. In these calculations, the exchange-correlation functional was the Revised PBE [21]. Among them, only the slab models containing some of nine elements were used as training data.

The NOMAD database contains a large number of cluster model results compared to other open databases. Only models that satisfy the following conditions were downloaded using the application programming interface:

1) Results from structure optimization of cluster models using VASP,
2) Calculated with the GGA-PBE exchange-correlation functional, and
3) Contain Ag, Au, Cu, Co, Ni, Ir, Pd, Pt, and/or Rh as metals.

The total energy after structure optimization for each model was used in this study. The adsorption energies of H and CO, denoted as ΔE_H and ΔE_{CO}, were calculated as follows.

$$\Delta E_H = E_{H^*} - E_* - \frac{1}{2}E_{H_2},$$
$$\Delta E_{CO} = E_{CO^*} - E_* - E_{CO},$$

where E_{H^*} and E_{CO^*} represent the total energies of the model after structure optimization with H and CO adsorbates, respectively, E_* is the total energy of the model without adsorbates, and E_{H_2} and E_{CO} are the total energies of H_2 and CO molecules in the gas phase. More negative adsorption energies indicate stronger interactions between the surface and the adsorbate.

B. MLPs

MLPs based on neural networks were created using the

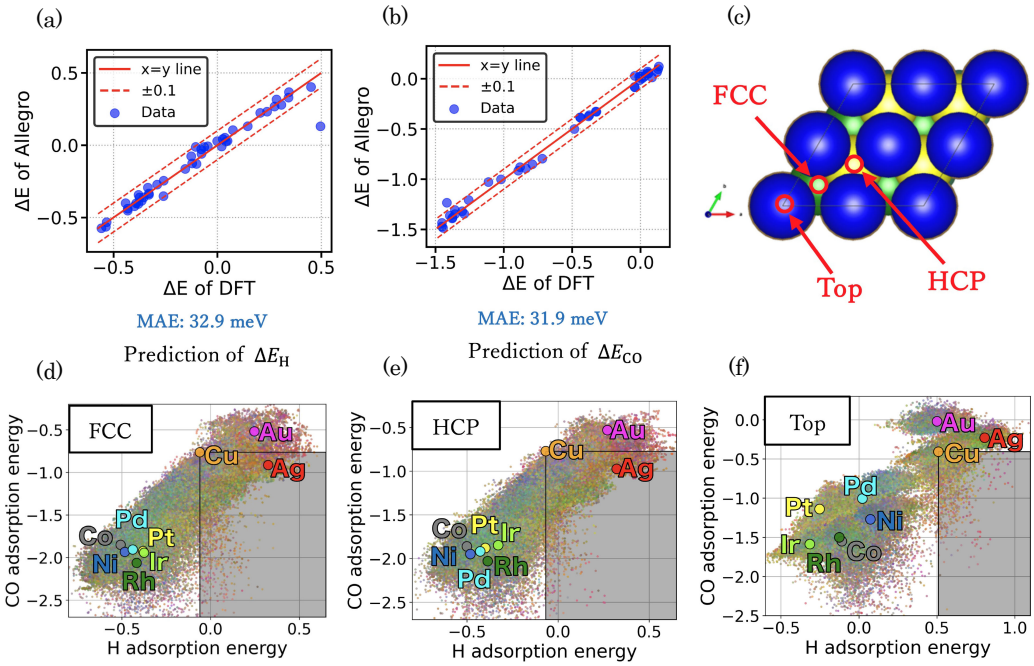

Figure 1: Prediction of (a) H atom adsorption energies and (b) CO molecular adsorption energies for the slab models. (c) Illustration of the three sites considered for the test data. Atoms in the topmost, second and third layers in the slab model are shown in blue, yellow, and light green, respectively. (d–f) Distribution of H atom and CO molecule adsorption energies at each site of 100,000 5-element slab models with randomly configured elements.

results of DFT calculations. The training data includes the element type Z, atomic position $\vec{r}$, and the total energy E.

In this study, we used Allegro, a recently developed graph neural network architecture built on the NequIP framework [22, 23]. Allegro demonstrates excellent accuracy and scalability, overcoming the drawbacks of conventional message passing neural network, such as high computational cost due to iterative information propagation. Details on hyperparameter settings in Allegro adopted in the present work are described in Supplementary Material.

III. RESULTS AND DISCUSSION

A. Prediction of adsorption energy for HEA slabs

First, using the results of DFT calculations of slab models [2, 15], we created MLPs to predict adsorption energies on HEA slabs. For this purpose, the training data included unary, binary, ternary, and quaternary alloys (17,007 data for H adsorption and 14,269 data for CO adsorption, with 8–80 atoms per supercell), as well as unary, quaternary, and quinary alloy slab models (960 data for H adsorption and 455 data for CO adsorption, with 21–22 atoms per supercell). To assess the prediction accuracy of the trained MLP, slab models containing five elements (45 data with 21–22 atoms per supercell) were used as test datasets. As shown in Figure 1(a, b), the accuracy of the created MLPs was high, with mean absolute errors (MAE) of 32.9 and 31.9 meV for the adsorption energies of H atoms and CO molecules, respectively.

These MLPs were used to predict the adsorption energies for additional five-element alloy slab models, including atomic species from the nine elements mentioned earlier. The lattice constant of each alloy was determined as a weighted average of the optimized bulk values of its constituent elements, as shown in Table S1 (Supplementary Material), based on the alloy composition. The distances of H and C from the surface were determined by the mode values obtained from datasets from the previous study [15], as shown in Figure S1 (Supplementary Material). Adsorption energies of H and CO were predicted at three sites (FCC, HCP, and Top), as shown in Figure 1(c), for 100,000 models with 20 atoms in a 2 × 2 supercell consisting of 5 layers. The results in Figure 1(d–f) represent the adsorption energies for H and CO. The colors indicate the ratio, with Ag-, Au-, Cu-, Co-, Ir-, Ni-, Pd-, Pt-, and Rh-rich compositions shown in red, pink, orange, gray, light green, blue, cyan, yellow, and green, respectively. The trends for the FCC and HCP sites are similar, while the Top site shows an overall increase in adsorption energy. Previous studies have reported a positive linear relationship between the adsorption energies of H and CO [24, 25]. However, our results indicate that this relationship does not necessarily hold for HEA surfaces. Notably, the darker regions in Figure 1(d–f) highlight areas where H adsorption is weaker and CO adsorption is stronger than that on a Cu surface, which is a desirable characteristic for CO_2RR catalysts. Many promising candidate materials are located within this region. We also demonstrated that high-throughput screening using MLPs enables the efficient identification of HEA models with the optimal adsorption energy ($\Delta E_{CO} = -0.67$ eV) [24] at a low computational cost.

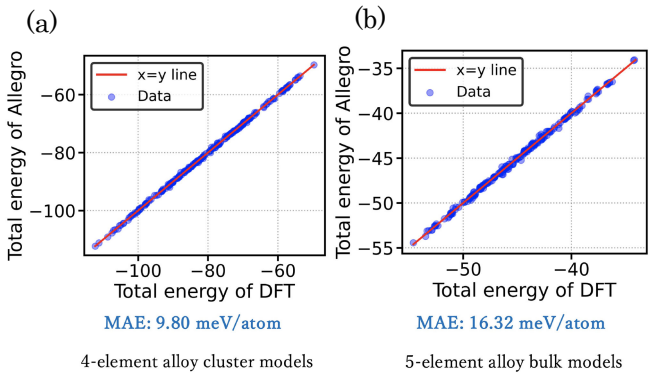

Figure 2: Prediction for (a) quaternary and (b) quinary systems using the model trained on DFT calculation data for unary to ternary systems.

B. Prediction for multi-element models

This section describes the investigation of catalysts using cluster models. First, DFT calculation results for unary-, binary-, and ternary-alloy models (3,969 data for cluster models and 741 data for bulk models) were used as training data. The trained MLP was then applied to predict the total energy of quaternary- and quinary-alloy model. As shown in Figure 2, the MLP accurately predicts the total energy for both bulk and cluster models (each 200 datasets), even for multi-element compositions not included in the training dataset. This demonstrates that the model effectively learns the relationship between different elements. This result is a significant milestone in reducing the computational cost of training multi-element models for two key reasons. First, generating DFT datasets for multi-element systems is challenging due to convergence difficulties. Second, existing open databases primarily contain crystal structures with only a limited number of elements.

C. Prediction for models of various shapes and sizes

As mentioned earlier, optimizing the shape and size of catalysts can enhance their activity and selectivity. Therefore, creating MLPs capable of predicting properties for cluster models with various shapes and sizes is crucial. The Alloy Catalysis Automated Toolkit [26] was used to generate unary models with octahedral, cubic, icosahedral, and spherical shapes (Figure 3) across various numbers of atoms, followed by structure optimization for each. MLPs were then trained to predict the energy of these models.

Initially, a pre-trained model specialized in catalyst design was used for predictions. Column I in Table 1 shows the prediction results using the GemNet-OC-S2EFS-OC20+OC22 model [27, 28]. This model was trained by GemNet on a large dataset from the Open Catalyst Project, which includes over 1,000,000 structure optimization snapshots. However, this model appears to be less effective when predicting the total energy of clusters with various shapes and sizes, indicating that the models trained on slab structures may not be the best fit for cluster models.

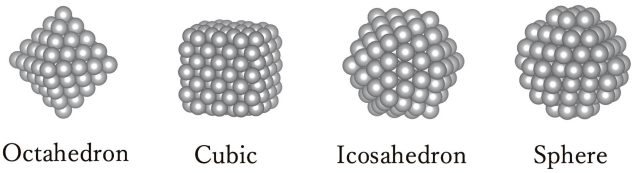

Figure 3: Type of shapes used in the test data. As regards size, the numbers of atoms listed in Table 1 were used to create structures.

Table 1: Predictions for models of various shapes and sizes using (I) the GemNet-OC-S2EFS-OC20+OC22 pre-trained model, (II) the Allegro trained with binary and ternary alloys in octahedral clusters consisting of 19 atoms (3,804 data), as well as with binary and ternary alloy bulk crystals (747 data), and (III) the Allegro trained with the datasets of (II) and randomly shaped unary clusters obtained from NOMAD (3,228 data).

Shape	Number of atoms	MAE (meV atom^{-1})			Number of test datasets
		I	II	III	
Octahedron	44	396.4	130.5	17.6	9
	85	446.6	150.9	15.0	9
Cubic	63	401.4	74.9	32.7	8
	171	449.7	88.9	26.9	8
Icosahedron	13	92.5	279.3	56.6	8
	55	420.7	97.6	13.1	7
	147	469.2	112.2	23.6	8
Sphere	135	456.4	107.2	19.6	8
	179	457.8	124.0	17.9	6

Column II in Table 1 shows the results of the Allegro model trained with binary and ternary alloys in octahedral cluster models consisting of 19 atoms (3,804 data), as well as with binary and ternary alloy bulk crystals (747 data). Except for the smallest icosahedral case, the accuracy of Allegro trained with clusters (II) is much better than that of the GemNet-OC-S2EFS-OC20+OC22 (I). This indicates that including certain cluster data in the training dataset lead to improved prediction performance for clusters with different sizes and shapes.

Column III in Table 1 shows the results of the Allegro model trained using the data from II, along with randomly shaped unary clusters consisting of 3–55 atoms obtained from NOMAD (3,228 data). The inclusion of these randomly shaped clusters significantly improves the accuracy across various cluster models. As a result, the MLP model in III is now well-suited for investigating the stability of a broad range of models.

IV. CONCLUSIONS

In this study, MLPs were developed based on limited DFT calculation datasets to explore a large configurational space of multi-element alloy catalysts by predicting the adsorption energies of H and CO. The analysis of slab models with these MLPs highlights the potential of HEAs as catalysts, with

adsorption energy values of ΔE_H and ΔE_{CO} that are highly correlated with CO_2RR catalytic activity, laying within the desirable range. Additionally, our MLPs also provides accurate predictions of total energies for models containing up to five elements, as well as cluster models with varying sizes and shapes, despite limited diversity in the training datasets.

Given the current limitations of DFT calculations for HEA clusters and the scarcity of available data, this study provides a promising foundation for future advancements in this field. For example, these MLPs serve as powerful tools for high-throughput screening of the optimal alloy compositions and optimizing the size and shape of cluster catalysts.

Acknowledgments

This work was supported by Japan Science and Technology Agency (JST) as part of SICORP, Grant Number JPMJSC21E2. Part of calculations were performed using the supercomputers at the Information Technology Center and the Institute for Solid State Physics (ISSP), the University of Tokyo.

Appendix

The details of hyperparameter settings in Allegro and predicted additional slab models in Figure 1(d–f) are available in Supplementary Material at https://doi.org/10.1380/ejssnt.2025-028.

Note 1

The data that support the findings of this study are available from the corresponding authors upon reasonable request.

Note 2

This paper was presented at the 10th International Symposium on Surface Science, Kitakyushu International Conference Center, Fukuoka, Japan, 20–24 October, 2024.

References

[1] T. K. Todorova, M. W. Schreiber, and M. Fontecave, ACS Catal. **10**, 1754 (2020).
[2] J. K. Pedersen, T. A. A. Batchelor, A. Bagger, and J. Rossmeisl, ACS Catal. **10**, 2169 (2020).
[3] S. Ma, M. Sadakiyo, R. Luo, M. Heima, M. Yamauchi, and P. J. A. Kenis, J. Power Sources **301**, 219 (2016).
[4] B. Cantor, I. T. H. Chang, P. Knight, and A. J. B. Vincent, Mater. Sci. Eng. A **375–377**, 213 (2004).
[5] J.-W. Yeh, S.-K. Chen, S.-J. Lin, J.-Y. Gan, T.-S. Chin, T.-T. Shun, C.-H. Tsau, and S.-Y. Chang, Adv. Eng. Mater. **6**, 299 (2004).
[6] M.-H. Tsai and J.-W. Yeh, Mater. Res. Lett. **2**, 107 (2014).
[7] T. Eom, W. J. Kim, H.-K. Lim, M. H. Han, K. H. Han, E.-K. Lee, S. Lebègue, Y. J. Hwang, B. K. Min, and H. Kim, J. Phys. Chem. C **122**, 9245 (2018).
[8] H. Tabassum, X. Yang, R. Zou, and G. Wu, Chem Catal. **2**, 1561 (2022).
[9] R. K. Raju, P. Rodriguez, and E. N. Brothers, Phys. Chem. Chem. Phys. **25**, 11630 (2023).
[10] X. Deng, D. Alfonso, T.-D. Nguyen-Phan, and D. R. Kauffman, ACS Catal. **13**, 15301 (2023).
[11] H. Mistry, R. Reske, Z. Zeng, Z.-J. Zhao, J. Greeley, P. Strasser, and B. R. Cuenya, J. Am. Chem. Soc. **136**, 16473 (2014).
[12] L. Gai, Y. K. Shin, M. Raju, A. C. T. van Duin, and S. Raman, J. Phys. Chem. C **120**, 9780 (2016).
[13] M. Rittiruam, P. Khamloet, A. Ektarawong, C. Atthapak, T. Saelee, P. Khajondetchairit, B. Alling, S. Praserthdam, and P. Praserthdam, Appl. Surf. Sci. **652**, 159297 (2024).
[14] S. Watanabe, W. Li, W. Jeong, D. Lee, K. Shimizu, E. Mimanitani, Y. Ando, and S. Han, J. Phys. Energy **3**, 012003 (2021).
[15] K. Tran and Z. W. Ulissi, Nat. Catal. **1**, 696 (2018).
[16] M. Scheidgen, L. Himanen, A. N. Ladines, D. Sikter, M. Nakhaee, Á. Fekete, T. Chang, A. Golparvar, J. A. Márquez, S. Brockhauser, S. Brückner, L. M. Ghiringhelli, F. Dietrich, D. Lehmberg, T. Denell, A. Albino, H. Näsström, S. Shabih, F. Dobener, M. Kühbach, R. Mozumder, J. F. Rudzinski, N. Daelman, J. M. Pizarro, M. Kuban, C. Salazar, P. Ondračka, H.-J. Bungartz, and C. Draxl, J. Open Source Softw. **8**, 5388 (2023).
[17] G. Kresse and J. Hafner, Phys. Rev. B **47**, 558(R) (1993).
[18] J. P. Perdew, K. Burke, and M. Ernzerhof, Phys. Rev. Lett. **77**, 3865 (1996).
[19] P. E. Blöchl, Phys. Rev. B **50**, 17953 (1994).
[20] H. J. Monkhorst and J. D. Pack, Phys. Rev. B **13**, 5188 (1976).
[21] B. Hammer, L. B. Hansen, and J. K. Nørskov, Phys. Rev. B **59**, 7413 (1999).
[22] A. Musaelian, S. Batzner, A. Johansson, L. Sun, C. J. Owen, M. Kornbluth, and B. Kozinsky, Nat. Commun. **14**, 579 (2023).
[23] S. Batzner, A. Musaelian, L. Sun, M. Geiger, J. P. Mailoa, M. Kornbluth, N. Molinari, T. E. Smidt, and B. Kozinsky, Nat. Commun. **13**, 2453 (2022).
[24] M. Zhong, K. Tran, Y. Min, C. Wang, Z. Wang, C.-T. Dinh, P. De Luna, Z. Yu, A. S. Rasouli, P. Brodersen, S. Sun, O. Voznyy, C.-S. Tan, M. Askerka, F. Che, M. Liu, A. Seifitokaldani, Y. Pang, S.-C. Lo, A. Ip, Z. Ulissi, and E. H. Sargent, Nature **581**, 178 (2020).
[25] H. Wan, X. Wang, L. Tan, M. Filippi, P. Strasser, J. Rossmeisl, and A. Bagger, ACS Catal. **13**, 1926 (2023).
[26] S. Han, G. Barcaro, A. Fortunelli, S. Lysgaard, T. Vegge, and H. A. Hansen, npj Comput. Mater. **8**, 121 (2022).
[27] R. Tran, J. Lan, M. Shuaibi, B. M. Wood, S. Goyal, A. Das, J. Heras-Domingo, A. Kolluru, A. Rizvi, N. Shoghi, A. Sriram, F. Therrien, J. Abed, O. Voznyy, E. H. Sargent, Z. Ulissi, and C. Lawrence Zitnick, ACS Catal. **13**, 3066 (2023).
[28] L. Chanussot, A. Das, S. Goyal, T. Lavril, M. Shuaibi, M. Riviere, K. Tran, J. Heras-Domingo, C. Ho, W. Hu, A. Palizhati, A. Sriram, B. Wood, J. Yoon, D. Parikh, C. L. Zitnick, and Z. Ulissi, ACS Catal. **11**, 6059 (2021).